Journal of Quantitative Spectroscopy & Radiative Transfer 340 (2025) 109444

Contents lists available at ScienceDirect

Journal of Quantitative Spectroscopy and Radiative Transfer

journal homepage: www.elsevier.com/locate/jqsrt

MARVEL analysis of high-resolution rovibrational spectra of $^{16}O^{12}C^{17}O$

Saja A.M. Obaidat [a,b], Ala'a A.A. Azzam [b,*], Dunia Alatoom [a,b,c], Mohammad Taha I. Ibrahim [a,c], Jonathan Tennyson [c,*], Tibor Furtenbacher [d], Attila G. Császár [d]

[a] Research Department, AstroJo Institute, Wasfi Al-Tal St, Amman, Jordan
[b] Department of Physics, The University of Jordan, Queen Rania St, Amman, Jordan
[c] Department of Physics and Astronomy, University College London, Gower Street, London WC1E 6BT, UK
[d] ELTE Eötvös Loránd University, Institute of Chemistry, H-1117 Budapest, Pázmány Péter sétány 1/A, Hungary

ARTICLE INFO

Keywords:
Rovibrational energy levels
CO_2
$^{16}O^{12}C^{17}O$
Line positions
Transitions
MARVEL

ABSTRACT

$^{16}O^{12}C^{17}O$ is the fourth most abundant isotopologue of carbon dioxide. As part of this study, a total of 16 223 rovibrational transitions, 9822 unique ones, measured for the ground electronic state of CO_2, were collected from 31 articles, corresponding to the limited wavenumber range of 634–12 727 cm^{-1}. The measured transitions span the polyads $P = 0–17$, where $P = 2v_1+v_2+3v_3$, and v_1, v_2, and v_3 are the normal-mode quantum numbers corresponding to the symmetric stretch, linear bend, and antisymmetric stretch motions. Following a careful validation of the compiled rovibrational transitions data, a set of 5036 empirical rovibrational energy levels has been determined. Comparison of the empirical energy-level data of this study with those in the CDSD-296 and NASA Ames-2021 line lists shows good general agreement.

1. Introduction

Despite being a symmetric linear molecule, carbon dioxide, CO_2, is one of the most important trace gases in the atmosphere of the Earth; indeed, it is second only to water in the HITRAN list [1] of molecules of atmospheric interest. The parent isotopologue, $^{16}C^{12}O_2$, is one of the most important anthropogenic climate-forcing agents; as such, it has particular relevance for the Earth's radiation budget. Thus, there have been several national and international missions [2–6] with the aim to quantify the amount and attribute the sources (*e.g.*, the oil and gas, waste, and energy sectors) of atmospheric CO_2.

The recent increase in the amount of CO_2 in the Earth's atmosphere, due mostly to the combustion of fossil fuels, impacts a number of natural systems and all living organisms in our ecosystem [7]. High-resolution rovibrational spectroscopy of isotopologues of carbon dioxide (*e.g.*, Refs. [1,8–18]) has also contributed to a better understanding of the nature of the atmospheres [19] of planets containing a significant amount of carbon dioxide, such as Venus [20] and Mars [21]. CO_2 has also been detected in exoplanet atmospheres [22].

There are multiple isotopic variants of CO_2, arising from the different combinations of the isotopes of the carbon and oxygen atoms:^{12}C, ^{13}C, ^{16}O, ^{17}O, and ^{18}O are the naturally occurring nuclides, though even $^{14}C^{16}O_2$ has been observed spectroscopically [9]. HITRAN lists 12 CO_2 isotopologues, it does not include radiocarbon $^{14}C^{16}O_2$. Isotopic abundances vary around the universe; thus, it is important to study the spectroscopy of all carbon dioxide isotopologues, not only the parent one, $^{12}C^{16}O_2$ (denoted 626 in HITRAN parlance, which we adopt here).

This paper focuses on rovibrational spectra measured, under various conditions by a number of different techniques, for the fourth most abundant carbon dioxide isotope, $^{16}O^{12}C^{17}O$ (HITRAN code 627). For 627 a significant number of high-resolution spectroscopic studies are available [8,23–52].

The parent 626 isotopologue forms 98.42% of naturally occurring carbon dioxide in the Earth's atmosphere. It is important to emphasize that the rovibrational bands of 626 are saturated in the Earth's atmosphere, meaning that increasing its concentration results in a logarithmic increase in absorption rather than the expected linear one [53]. Isotopic substitution within carbon dioxide can result in absorptions shifted into windows where the absorption is indeed linearly related to concentration; this is particularly true for the much less abundant asymmetrically substituted CO_2 isotopologues, such as 627 (with a natural abundance of 0.07%). One of the effects of symmetry breaking is that all rotational states are allowed for 627, in contrast to 626, for which half of the states are forbidden by the Pauli principle, leading to a roughly fourfold increase in the number of transitions. The (ro)vibrational selection rules also change with all vibrational (and even pure rotational) transitions now formally allowed, although

---

* Corresponding authors.
E-mail addresses: alaa.azzam@ju.edu.jo (A.A.A. Azzam), j.tennyson@ucl.ac.uk (J. Tennyson).

https://doi.org/10.1016/j.jqsrt.2025.109444
Received 28 January 2025; Received in revised form 16 March 2025; Accepted 17 March 2025

transitions forbidden in 626 generally remain weak in 627. In summary, asymmetric isotopologues of CO_2 have significantly more spectral lines than 626 and, importantly, lines in regions where 626 absorption is not dominant.

The main goal of this study is to provide two expansive spectroscopic datasets for the carbon dioxide isotope 627. The first one includes accurately measured, validated line positions with unique lower- and upper-state labels, while the second contains empirical rovibrational energies with experiment-based uncertainties. Determination of the energy levels from the measured transitions is accomplished through the use of the MARVEL (Measured Active Rotational–Vibrational Energy Levels) procedure [54–58], which is based on the theory of spectroscopic networks [59,60]. The resulting datasets can be used to improve line lists such as those provided by HITRAN [61], NASA Ames [13,62] and ExoMol [63], and can support the refinement of the potential energy surfaces used in variational nuclear motion calculations. This work is part of our investigation of the spectroscopy of carbon dioxide isotopologues, with results published for 626 [18], 636 [14], 628 [15], 638 [17], and 838, 728, and 828 [16].

2. Theoretical background

2.1. MARVEL

MARVEL [54–58,64] is a tool which can be used to efficiently analyze measured high-resolution spectroscopic transitions and use the validated ones to determine empirical energy levels. It works through the construction of a “spectroscopic network” (SN) [59,60], where the energy levels are the vertices and the transitions between them are the edges. When input transitions are collected for a MARVEL analysis, one must ensure that each line has an accurate center position with an associated (extended) uncertainty, and that the upper and lower energy levels involved in the transition are labeled uniquely. Based on the spectroscopic network created, MARVEL can identify most of the inconsistencies in the input data set and, based on the validated transitions, it yields empirical energy levels through an inversion protocol. In cases where the experimental data are highly incomplete, the network may become fragmented, leaving some energy levels isolated from the component containing the root (the lowest-energy quantum state of the molecule) of the SN. These so-called “floating components” can be connected to the root and the measured transitions using sufficiently accurate empirical data (coming from perhaps effective Hamiltonian fits) or, for some molecules, by using the known quasi-degeneracy of certain energy levels [65].

Unlike quantum-chemical models based on the nuclear Hamiltonian, culminating in the solution of the corresponding nuclear Schrödinger equation, the accuracy of the empirical (MARVEL) energy levels is not restricted by assumptions other than the validity of the Ritz principle [66] and, of course, the accuracy of the measurements. This allows maintaining experimental accuracy during a MARVEL determination of energy levels. The only significant caveat about not knowing details of quantum mechanics is that it also allows MARVEL to accept transitions that might break standard selection rules or are incorrect otherwise, as long as the transition is not in conflict with the other entries of the dataset.

In this study, we used the latest version of the MARVEL code, MARVEL4 [64]. MARVEL4 has an option to use an adaptation of the bootstrap method to give final uncertainties for the energy levels; our final energy levels are given with uncertainties obtained using this procedure.

2.2. Rovibrational quantum numbers

To ensure that the validation of the measured transitions offered by MARVEL is correct, it is crucial that the labeling of the energy levels is consistent throughout the dataset. In this study, as in our previous investigations of the isotopologues 636 [14], 628 [15], (828, 728, 838) [16], (638) [17], and (626) [18], we employ the AFGL (Air Force Geophysics Laboratory) notation [67–69] to describe the vibrational quantum states of CO_2. This notation utilizes a number of descriptors and avoids the use of super- and subscripts, making it ideal for electronic databases. The vibrational states are represented by four quantum numbers: v_1 and v_3 correspond to the symmetric and antisymmetric stretches, v_2 denotes the (doubly degenerate) bending mode, and l_2 represents the angular momentum linked to the bending mode. Additionally, the ranking index r refers to the Fermi resonances complicating the spectra of carbon dioxide [67] (r ranges from 1 to v_1+1 [69–71]). See Fig. 1 for the distribution of r across the experimental wavenumber range covered in this study (corresponding to the range covered by experiments; there is a single source, 13PaLiLuLi [52], with transitions measured above 8300 cm^{-1}).

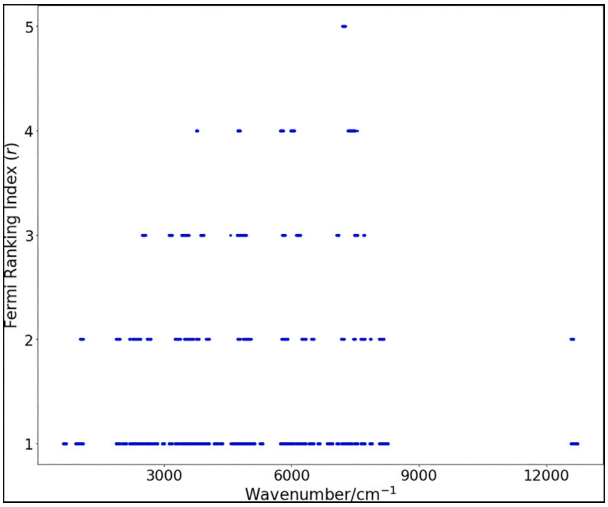

Fig. 1. Distribution of the Fermi ranking index, r, of the empirical energy levels of $^{16}O^{12}C^{17}O$ across the experimental wavenumber range covered in this study.

Unlike for most molecules, for CO_2 several polyad numbers (defined as a simple sum of normal-mode quantum numbers multiplied by positive weights) have been proposed [72–75] to help interpret the vibrational energy-level structure of this molecule. The choice made here is $P = 2v_1 + v_2 + 3v_3$, following again the AFGL notation.

In addition to the five vibrational descriptors, two further descriptors are used to characterize the rovibrational quantum states of CO_2: the rotational quantum number J and the rotationless parity p, labeled either ‘e’ or ‘f’ [76]. Thus, the complete label for a rovibrational quantum state of 627, similar to all the other carbon dioxide isotopologues, is $(J\ v_1\ v_2\ l_2\ v_3\ r\ p)$.

It is important to note that in the AFGL notation the quantum numbers v_2 and l_2 are always identical [77]. The advantage of the AFGL system, as first demonstrated by Amat and Pimbert [67], is that unlike the standard notation, where the order of rovibrational energy levels may shift between isotopologues, this does not occur in the AFGL system; the price to pay is the introduction of a redundant descriptor.

Non-degenerate vibrational states with $v_2 = l_2 = 0$ always have parity e; therefore, in some literature sources, the parity information is not explicitly stated. Vibrational states with $l_2 > 0$ support both e- and f-parity states for each J. Finally, we note that $J \geq l_2$, meaning, for example, that there is no $J = 0$ level for vibrational states with $l_2 > 0$.

2.3. Selection rules

For all asymmetric CO_2 isotopologues, the equilibrium geometry belongs to the $C_{\infty v}$ point group, which means that there are no formal selection rules on the vibrational transitions. The selection rules

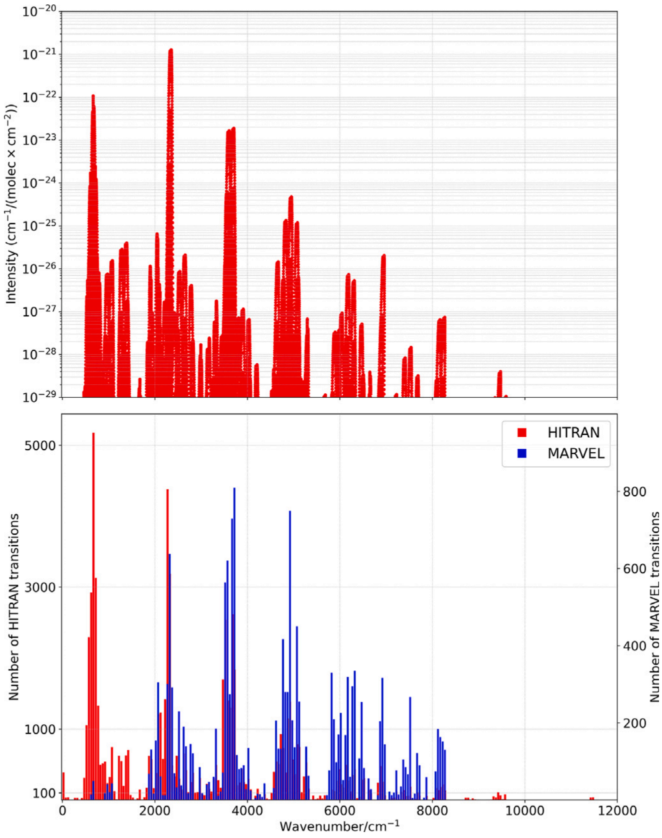

Fig. 2. Comparison of the data provided by HITRAN [61] with our collected experimental transitions. The upper plot shows the distribution of HITRAN transitions and their intensities; intensities are scaled by the natural abundance of $^{16}O^{12}C^{17}O$ as this is the HITRAN convention. The lower plot shows a bar comparison between the number of transitions available in HITRAN (left-hand scale) with the smaller number of transitions available in our MARVEL dataset (right-hand scale); each bar gives the number of transitions in a bin of 50 cm^{-1}.

for one-photon, dipole-allowed rovibrational transitions among the rovibrational quantum states of 627 are summarized in what follows.

For rotational transitions, the usual dipole selection rule is $\Delta J = 0, \pm 1$, and when

$$\Delta J = 0; \quad e \leftrightarrow f, \tag{1}$$

meaning that the rotationless parity changes between the initial and the final states in the Q branch, whereas when

$$\Delta J = \pm 1; \quad e \leftrightarrow e, \quad f \leftrightarrow f, \tag{2}$$

indicating no parity change in the P and R branches.

3. Experimental studies of$^{16}O^{12}C^{17}O$ line positions

3.1. Literature sources utilized

The input file “transitions_627.txt” used during the MARVEL analysis is part of the Supplementary Material, and it contains 16 223 input transitions, collected from 31 sources. In this file, each transition is characterized by (a) a line position (in units that are indicated in the segment file), (b) an initial and an adjusted, expanded (two-sigma) uncertainty for the line position (the adjusted uncertainty is the one which ensures that the present set of input transitions is self-consistent), (c) the rovibrational assignments of the upper and lower states (see Section 2.2 for a description of the labels of the quantum states and Section 2.3 for the selection rules), and (d) a line tag, a metadata string providing a unique identifier (for multi-author publications, each tag contains the last two digits of the year of the publication and the first two characters of the last names of the authors, up to the first four authors) plus a sequence number for each line.

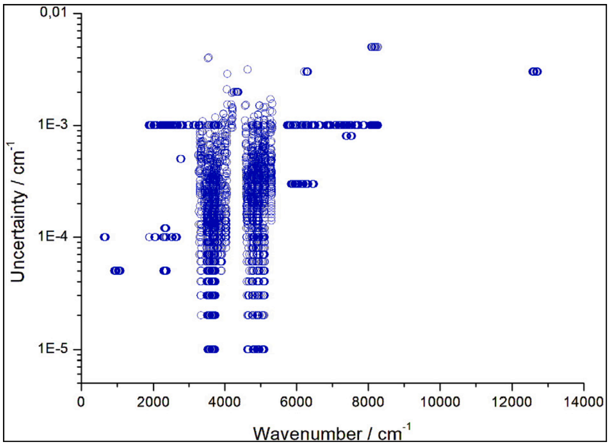

Fig. 3. Expanded (two-sigma) uncertainties of the experimental rovibrational line-center positions collected, as a function of the transition wavenumber (note the logarithmic scale of the vertical axis). If multiple measurements are available for the same line, the most accurate one is shown.

Characteristics of the 31 literature sources containing the transitions collected are summarized in Table 1. The wavenumber range covered by these measurements is limited to 634 – 12 727 cm^{-1} (see Fig. 2). Of all the experimentally measured transitions, only about half of them, 9822, are unique, which means that on average each transition has been measured twice. Fig. 2 shows that the number of transitions considered important enough to include in HITRAN is considerably greater than the number actually measured in the laboratory and used in our MARVEL study; in practice, the HITRAN transition wavenumbers for 627 are cited as coming from theoretical sources [78–80]. Fig. 2 also shows areas where it should be possible to observe further spectra, while highlighting that most of the gaps in our transitions are due to transparency windows. Specifically, the range below 2000 cm^{-1} and above 9000 cm^{-1} could benefit from experimental studies.

Fig. 3 shows the final, adjusted, expanded (two-sigma) experimental uncertainties of the validated rovibrational transition measurements of $^{16}O^{12}C^{17}O$ as a function of the transition wavenumber (to make the spectroscopic network of $^{16}O^{12}C^{17}O$ self-consistent, some of the reported uncertainties had to be slightly adjusted). This figure conveys the following information: (a) the experimental uncertainties cover almost three orders of magnitude, from 10^{-5} to 10^{-2} cm^{-1}, (b) the wavenumber range covered by the experiments is rather limited, only going up to 13 000 cm^{-1}, and (c) there are no measurements between about 9000–12 000 cm^{-1}.

3.2. *Specific comments on entries of Table 1*

It is a tribute to the careful experimental investigations of the high-resolution spectra of the 627 isotopologue of carbon dioxide that during the MARVEL analysis only 103 transitions had to be removed from the spectroscopic network assembled. These suspicious transitions are indicated with a negative sign in front of the transition wavenumber entry in the file “transitions_627.txt”.

The source 16BeDeSuBr [39] provides the majority of the problematic transitions with 75 transitions incompatible with the rest of the data. Most of the rejected transitions of this source have large uncertainties, 0.01–0.02 cm^{-1}. We note that a significant number of transitions from this source also had to be deleted during the investigation of the 636 [14] and 628 [15] isotopologues. There are three further sources with a significant number of deleted transitions: 13, 7, and

Table 1
^{16}O^{12}C^{17}O data sources used in this work and their characteristics, including the number of measured (A), floating (F), validated (V), and deleted (D) transitions. U^{CSU} is the average expanded 'claimed source uncertainty', and U^{MSU} is the average expanded 'MARVEL-suggested source uncertainty'.

Source	Range/cm^{-1}	$A/F/V/D$	U^{CSU}	U^{MSU}
80PaKaAn [25]	634.40–696.46	63/0/63/0	1.0×10^{-4}	1.6×10^{-3}
99ClTeHuVa [28]	919.41–1098.73	122/0/122/0	5.0×10^{-5}	7.4×10^{-5}
12LyKaJaLu [29]	1872.69–8269.65	5675/51/5617/7	1.0×10^{-3}	1.2×10^{-3}
84RiBeDeFe [30]	1885.61–2674.83	269/0/269/0	1.0×10^{-3}	1.5×10^{-3}
12JaGuLyKa [31]	1887.06–5107.12	500/0/500/0	1.0×10^{-4}	1.1×10^{-4}
85RiBeDe [32]	1887.06–1917.46	17/0/17/0	5.0×10^{-2}	5.0×10^{-2}
84RiBe [26]	2024.43–2073.53	29/0/29/0	1.0×10^{-3}	1.1×10^{-3}
86RiBeDe [27]	2086.89–2089.85	3/0/3/0	1.0×10^{-3}	1.5×10^{-3}
14ElSuMi [33]	2280.79–2377.01	83/0/82/1	5.0×10^{-5}	5.5×10^{-5}
78BaDeChRa [23]	2283.03–2372.81	121/0/121/0	3.0×10^{-3}	4.0×10^{-3}
80Guelachv [24]	2305.10–2365.89	81/0/81/0	1.2×10^{-4}	3.9×10^{-4}
84DeRiBe [34]	2494.81–2674.12	127/0/127/0	2.0×10^{-3}	2.1×10^{-3}
08ViMuNoHe [35]	2753.48–2787.89	43/0/30/13	5.0×10^{-4}	4.1×10^{-3}
14BoJaLyTa [36]	3260.70–4678.67	2612/96/2516/0	1.6×10^{-4}	2.7×10^{-4}
16VaKoMoKa [37]	4248.20–4378.20	71/1/70/0	2.0×10^{-3}	3.3×10^{-3}
15BoJaLyTa [38]	4715.45–5318.23	1640/0/1635/5	2.1×10^{-4}	4.0×10^{-4}
16BeDeSuBr [39]	4775.00–4933.10	230/0/155/75	3.0×10^{-4}	2.1×10^{-3}
19MoKaPeTa [40]	5732.83–5850.04	265/0/265/0	1.0×10^{-3}	1.0×10^{-3}
18KaCeMoKa [41]	5787.23–5908.92	165/0/165/0	1.0×10^{-3}	1.1×10^{-3}
18CeKaMoKa [42]	5801.61–5878.10	87/0/87/0	1.0×10^{-3}	1.2×10^{-3}
15JaBoLyTa [43]	5841.21–6493.30	658/0/658/0	3.0×10^{-4}	4.8×10^{-4}
14KaCaMoKa [44]	5857.65–6961.20	1000/0/999/1	1.0×10^{-3}	1.1×10^{-3}
08PeKaPeTa [8]	5859.82–6961.21	264/0/264/0	1.0×10^{-3}	1.6×10^{-3}
06PeKaRoPe [45]	5957.20–6171.11	135/0/135/0	1.1×10^{-3}	1.7×10^{-3}
05MaMaRoPe [46]	6206.10–6494.52	254/0/254/0	3.0×10^{-3}	3.3×10^{-3}
17KaKaTaPe [47]	7056.76–7896.71	811/0/811/0	1.0×10^{-3}	1.1×10^{-3}
09KaSoCa [48]	7371.28–7549.96	96/0/95/1	8.0×10^{-4}	9.6×10^{-4}
10SoKaTaPe [49]	7371.28–7550.36	96/0/96/0	1.0×10^{-3}	1.0×10^{-3}
14KaKaTaPe [50]	8058.36–8269.86	303/0/303/0	1.0×10^{-3}	1.1×10^{-3}
13GoHeLy [51]	8079.19–8270.08	264/0/264/0	5.0×10^{-3}	5.3×10^{-3}
13PaLiLuLi [52]	12 572.86–12 726.69	140/0/140/0	3.0×10^{-3}	3.0×10^{-3}

5 transitions were deleted from 08ViMuNoHe [35], 12LyKaJaLu [29], and 15BoJaLyTa [38], respectively. These lines show a discrepancy of more than 0.02 cm^{-1} when compared to CDSD-296 [10] and NASA Ames-2021 [13]; as a result, they were excluded from further analysis.

4. Results and discussion

4.1. Energy levels

The empirical energy values, obtained in this study for 5036 rovibrational states in the 0 – 13 469 hc cm^{-1} range, are available in the file "Energylevels_627.txt". Each energy level of this data file is characterized by (a) a rovibrational label, (b) an empirical (MARVEL) energy (in hc cm^{-1}), (c) an expanded (two-sigma) energy uncertainty (in hc cm^{-1}), and (d) the number of transitions incident to this state.

The energy-level coverage of the dataset obtained during this study against that of NASA Ames-2021 [13] can be ascertained from Fig. 4. The analysis again reveals a significant lack of experimental data above 10 000 cm^{-1}, particularly at high J values (J beyond about 80), with a notable gap above about 8000 cm^{-1}. These observations highlight the need for laboratory measurements conducted at elevated temperatures.

The distribution of the number of transitions linking to each energy level is shown, as a function of the empirical rovibrational energy, in Fig. 5. Fig. 5 reflects the fact that in experimental spectroscopic networks the degrees of the quantum states display an inverse-power-law-like (*i.e.*, heavy-tailed or near scale-free [81]) distribution [57,82]. This distribution implies the presence of a small number of high-degree, quantum states, called hubs. The highest-degree hubs of 627, which have more than 175 incident transitions, are all in the vibrational ground state, with $J = 8$–15 and 17–24, where it is interesting to see that $J = 16$ is not in the list. As illustrated in Fig. 5, 1178 out of the 5036 levels determined in this study are determined by a single transition. Empirical energy levels derived from (or connected by) a single transition are considered to be inherently less reliable than those determined by multiple measured transitions. Nevertheless, our comparisons with other compilations of 627 energy levels, see below, did not identify any issues, suggesting that these levels are reliable.

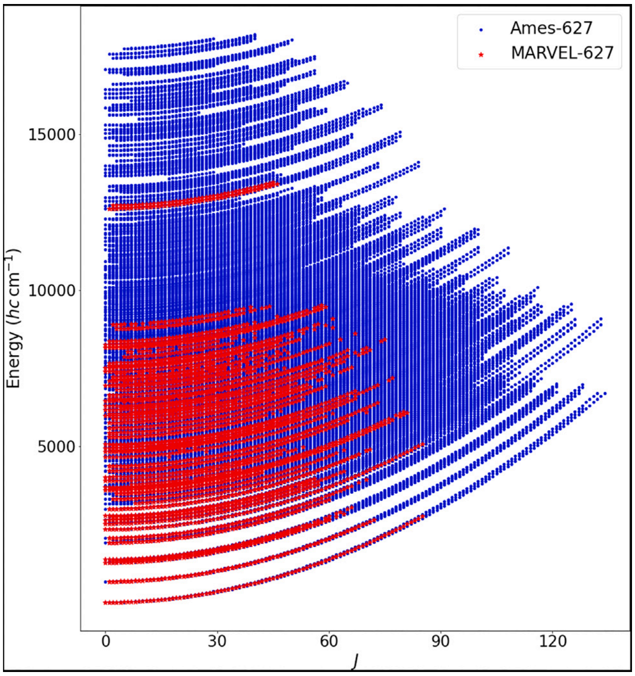

Fig. 4. Energy-level coverage of the dataset obtained during this study (red dots) against that of NASA Ames-2021 [13] (blue dots). See Table 3 for details about the vibrational bands of ^{16}O^{12}C^{17}O.

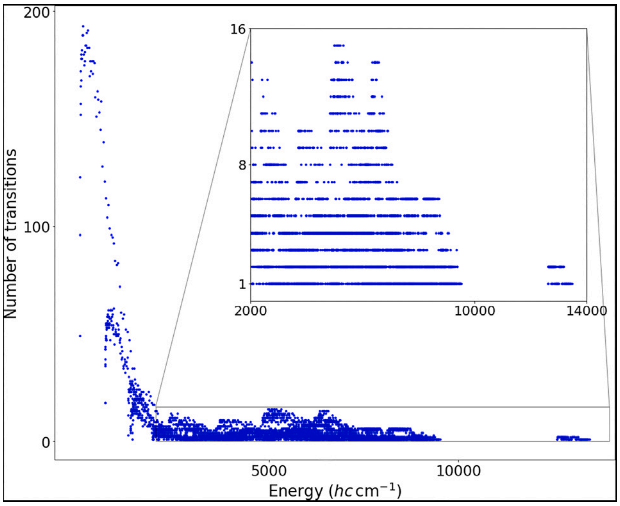

Fig. 5. Distribution of the number of incident transitions on the empirical rovibrational energy levels of $^{16}O^{12}C^{17}O$.

Table 2
Experimentally determined vibrational band origins (VBO) of $^{16}O^{12}C^{17}O$ with expanded (two-sigma) uncertainties (Unc.) and those of CDSD-296 [10]. All energy data in $hc\,\mathrm{cm}^{-1}$.

Band	MARVEL	Unc.	CDSD-296
(0 0 0 0 1 *e*)	0.00000	0.00000	0.00000
(1 0 0 0 2 *e*)	1272.28674	0.00100	1272.28650
(1 0 0 0 1 *e*)	1376.02508	0.00027	1376.02737
(0 0 0 1 1 *e*)	2340.01354	0.00030	2340.01336
(2 0 0 0 3 *e*)	2524.24782	0.00104	2524.24811
(2 0 0 0 2 *e*)	2641.24017	0.00104	2641.24039
(2 0 0 0 1 *e*)	2775.59149	0.00104	2775.59215
(1 0 0 1 2 *e*)	3591.26949	0.00027	3591.26967
(1 0 0 1 1 *e*)	3693.35646	0.00027	3693.35657
(3 0 0 0 3 *e*)	3898.24483	0.00071	3898.24561
(3 0 0 0 2 *e*)	4023.41806	0.00120	4023.41820
(0 0 0 2 1 *e*)	4655.20279	0.00029	4655.20268
(2 0 0 1 3 *e*)	4821.51468	0.00027	4821.51464
(2 0 0 1 2 *e*)	4939.36168	0.00027	4939.36183
(2 0 0 1 1 *e*)	5068.92488	0.00027	5068.92479
(1 0 0 2 1 *e*)	5986.12898	0.00104	5986.12883
(3 0 0 1 3 *e*)	6175.95108	0.00041	6175.95141
(3 0 0 1 2 *e*)	6298.11211	0.00041	6298.11219
(3 0 0 1 1 *e*)	6463.47948	0.00104	6463.48047
(0 0 0 3 1 *e*)	6945.59751	0.00104	6945.59729
(4 0 0 1 4 *e*)	7397.75798	0.00104	7397.75716
(4 0 0 1 3 *e*)	7525.82098	0.00104	7525.82035
(1 0 0 3 2 *e*)	8154.46303	0.00104	8154.46307
(1 0 0 3 1 *e*)	8254.38997	0.00501	8254.39116

Table 2 presents the experimentally determined vibrational band origins (VBO) for the $^{16}O^{12}C^{17}O$ isotopologue. The vibrational quantum numbers are listed in the first column, fully specifying the vibrational states. The VBO's, provided in cm^{-1}, correspond to empirical energy levels with $J = 0$ and $l_2 = 0$. Determining the energies of states with $l_2 > 0$ requires some fitting procedure, which is beyond the scope of this work. The values of Table 2 are derived from the set of empirical energy levels determined through MARVEL. Note also that the agreement with the CDSD-296 values is perfect, well within the expanded uncertainties of the empirical (MARVEL) energy levels.

Fig. 6 illustrates the distribution of all the empirical rovibrational energy levels of 627, grouped according to the polyad number $P = 2v_1 + v_2 + 3v_3$. This figure shows clearly the occasional ambiguities related to the definition of P.

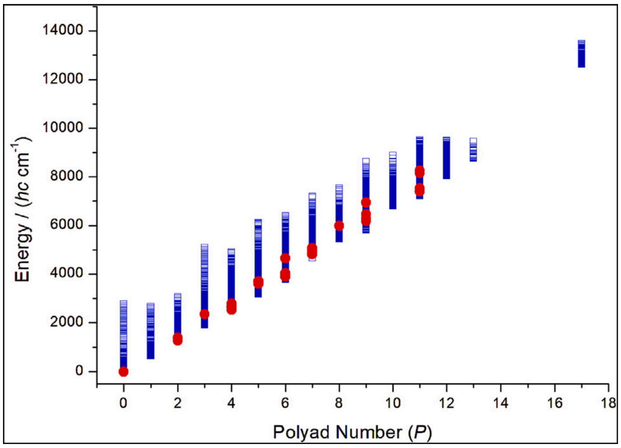

Fig. 6. Empirical rovibrational energy levels of $^{16}O^{12}C^{17}O$ grouped by the polyad number $P = 2v_1 + v_2 + 3v_3$. The vibrational band origins (see Table 2 for their complete list) are given as red dots.

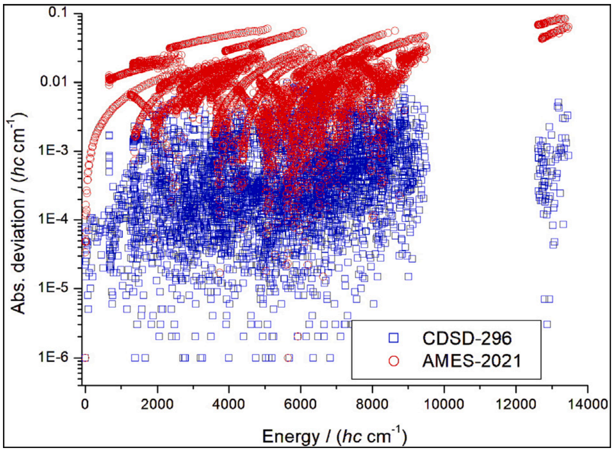

Fig. 7. Comparison between rovibrational energies of the present $^{16}O^{12}C^{17}O$ dataset and those of CDSD-296 [10] (blue squares) and NASA Ames-2021 [13] (red circles).

4.2. Comparison with line lists

Fig. 7 shows the absolute differences between the empirical (MARVEL) energy levels data and those of CDSD-296 [10] and NASA Ames-2021 [13] line lists. The MARVEL data show significantly better agreement with CDSD-296 (with a root-mean-square, rms, deviation of 0.0014 $hc\,\mathrm{cm}^{-1}$) than with unadjusted NASA Ames-2021 levels computed using the Ames-2 potential energy surface (the rms value is 0.0165 $hc\,\mathrm{cm}^{-1}$). This is not surprising, as the CDSD-296 data are semi-empirical in nature, they were generated from effective Hamiltonian models accurately fitted to experimental data available prior to 2019. These comparisons provide extra validation to the MARVEL energy levels of this study.

5. Summary and conclusions

This study presents a comprehensive analysis of all the available high-resolution, rovibrational transitions of the fourth most abundant isotopologue of carbon dioxide, $^{16}O^{12}C^{17}O$. For this analysis, the MARVEL algorithm and code [54–56] were employed. The transitions forming the basis of the MARVEL analysis were collected from 31 literature sources. The 16 223 measured transitions collected cover the wavenumber range of 634–12 727 cm^{-1}. The number of unique transitions this database contains is 9822. Just 103 of all the transitions collected had

Table 3

Vibrational bands of $^{16}O^{12}C^{17}O$ investigated in this study, with the ordering based on band descriptors (without the rotational quantum number J). Vibrational band origins (VBO) with "–" referring to VBOs which could not be directly determined from the present dataset of measured transitions.

Band	Range of J	No. of energy levels	Unc. range/hc cm^{-1}	Avg. unc./hc cm^{-1}	Range of energy levels/hc cm^{-1}	VBO/hc cm^{-1}
(0 0 0 0 1 e)	0–85	86	0.0000–0.0028	0.0004	0.00–2760.96	0.00
(0 0 0 1 1 e)	0–85	86	0.0001–0.0030	0.0005	2340.01–5079.18	2340.01354(30)
(0 0 0 2 1 e)	0–61	61	0.0002–0.0009	0.0002	4655.20–6062.78	4655.20279(29)
(0 0 0 3 1 e)	0–67	63	0.0010–0.0010	0.0010	6945.60–8627.23	6945.59751(104)
(0 1 1 0 1 e)	1–72	72	0.0002–0.0027	0.0005	665.49–2653.40	–
(0 1 1 0 1 f)	1–69	69	0.0002–0.0032	0.0006	665.49–2495.28	–
(0 1 1 1 1 e)	1–71	70	0.0002–0.0031	0.0010	2993.05–4911.50	–
(0 1 1 1 1 f)	1–70	69	0.0002–0.0035	0.0011	2993.06–4861.06	–
(0 1 1 2 1 e)	1–47	44	0.0002–0.0016	0.0004	5295.82–6136.21	–
(0 1 1 2 1 f)	1–45	44	0.0001–0.0010	0.0004	5295.83–6068.04	–
(0 1 1 3 1 e)	1–46	45	0.0010–0.0015	0.0011	7573.83–8372.82	–
(0 1 1 3 1 f)	1–59	52	0.0010–0.0019	0.0011	7573.84–8883.81	–
(0 2 2 0 1 e)	2–59	55	0.0010–0.0018	0.0012	1332.12–2673.47	–
(0 2 2 0 1 f)	2–51	49	0.0011–0.0032	0.0015	1332.12–2336.76	–
(0 2 2 1 1 e)	2–58	55	0.0001–0.0020	0.0010	3647.26–4933.85	–
(0 2 2 1 1 f)	2–50	47	0.0015–0.0037	0.0018	3647.26–4605.72	–
(0 2 2 2 1 f)	18–18	1	0.0017–0.0017	0.0017	6063.32–6063.32	–
(0 2 2 3 1 e)	7–34	14	0.0014–0.0016	0.0015	8221.82–8642.59	–
(0 2 2 3 1 f)	7–34	14	0.0015–0.0017	0.0015	8221.82–8642.60	–
(1 0 0 0 1 e)	0–66	63	0.0000–0.0010	0.0003	1376.03–3048.89	1376.02508(27)
(1 0 0 0 2 e)	0–64	63	0.0000–0.0010	0.0003	1272.29–2845.16	1272.28674(100)
(1 0 0 1 1 e)	0–80	80	0.0000–0.0015	0.0002	3693.36–6123.76	3693.35646(27)
(1 0 0 1 2 e)	0–81	81	0.0000–0.0020	0.0003	3591.27–6080.96	3591.26949(27)
(1 0 0 2 1 e)	0–49	48	0.0003–0.0010	0.0005	5986.13–6898.65	5986.12898(104)
(1 0 0 2 2 e)	2–66	60	0.0003–0.0013	0.0007	5887.56–7531.52	–
(1 0 0 3 1 e)	0–58	58	0.0010–0.0050	0.0016	8254.39–9518.20	8254.38997(501)
(1 0 0 3 2 e)	0–59	60	0.0010–0.0050	0.0016	8154.46–9462.58	8154.46303(104)
(1 0 0 5 1 e)	2–45	44	0.0030–0.0030	0.0030	12 719.78–13 469.81	–
(1 0 0 5 2 e)	1–46	46	0.0030–0.0030	0.0030	12 618.88–13 405.10	–
(1 1 1 0 1 e)	1–70	68	0.0001–0.0041	0.0008	2062.86–3942.52	–
(1 1 1 0 1 f)	1–53	53	0.0001–0.0039	0.0008	2062.86–3148.28	–
(1 1 1 0 2 e)	1–60	60	0.0001–0.0010	0.0006	1917.45–3302.10	–
(1 1 1 0 2 f)	1–52	51	0.0002–0.0012	0.0006	1917.45–2962.59	–
(1 1 1 1 1 e)	1–73	73	0.0002–0.0027	0.0005	4367.55–6394.48	–
(1 1 1 1 1 f)	1–70	69	0.0002–0.0032	0.0006	4367.56–6236.90	–
(1 1 1 1 2 e)	1–65	64	0.0002–0.0011	0.0003	4224.17–5834.59	–
(1 1 1 1 2 f)	1–70	63	0.0002–0.0033	0.0005	4224.18–6093.53	–
(1 1 1 2 1 e)	1–45	39	0.0010–0.0023	0.0011	6647.68–7418.61	–
(1 1 1 2 1 f)	1–48	40	0.0010–0.0010	0.0010	6647.69–7525.58	–
(1 1 1 2 2 e)	1–58	53	0.0010–0.0016	0.0011	6506.05–7781.04	–
(1 1 1 2 2 f)	1–56	52	0.0010–0.0019	0.0011	6506.05–7697.99	–
(1 1 1 3 1 e)	2–39	26	0.0010–0.0034	0.0011	8904.78–9479.58	–
(1 1 1 3 1 f)	2–36	25	0.0010–0.0036	0.0011	8904.78–9396.30	–
(1 1 1 3 2 e)	3–44	35	0.0010–0.0050	0.0014	8766.80–9495.22	–
(1 1 1 3 2 f)	3–40	34	0.0010–0.0050	0.0016	8766.81–9370.78	–
(1 2 2 0 1 e)	2–56	53	0.0010–0.0015	0.0010	2745.68–3955.05	–
(1 2 2 0 1 f)	2–55	53	0.0010–0.0018	0.0011	2745.68–3912.75	–
(1 2 2 1 1 e)	2–53	50	0.0010–0.0018	0.0011	5037.78–6113.67	–
(1 2 2 1 1 f)	2–50	49	0.0011–0.0032	0.0014	5037.78–5996.33	–
(1 2 2 1 2 e)	2–54	49	0.0010–0.0019	0.0011	4863.33–5980.45	–
(1 2 2 1 2 f)	2–50	46	0.0011–0.0032	0.0014	4863.32–5822.25	–
(1 2 2 2 2 e)	2–38	17	0.0014–0.0016	0.0015	7132.99–7685.42	–
(1 2 2 2 2 f)	5–47	19	0.0015–0.0033	0.0017	7141.98–7974.85	–
(2 0 0 0 1 e)	0–56	57	0.0005–0.0015	0.0010	2775.59–3985.29	2775.59149(104)
(2 0 0 0 2 e)	0–64	65	0.0001–0.0010	0.0005	2641.24–4211.86	2641.24017(104)
(2 0 0 0 3 e)	0–57	58	0.0001–0.0010	0.0005	2524.2–3776.07	2524.24782(104)
(2 0 0 1 1 e)	0–67	68	0.0000–0.0008	0.0002	5068.92–6781.32	5068.92488(27)
(2 0 0 1 2 e)	0–77	75	0.0000–0.0015	0.0002	4939.36–7187.93	4939.36168(27)
(2 0 0 1 3 e)	0–67	68	0.0000–0.0014	0.0002	4821.51–6532.86	4821.51468(27)
(2 0 0 2 1 e)	3–37	18	0.0010–0.0013	0.0010	7342.35–7862.49	–
(2 0 0 2 2 e)	2–48	37	0.0010–0.0018	0.0010	7215.13–8087.46	–
(2 0 0 2 3 e)	1–49	41	0.0010–0.0019	0.0011	7094.57–8008.07	–
(2 1 1 0 1 e)	3–42	40	0.0001–0.0013	0.0008	3480.18–4159.76	–
(2 1 1 0 1 f)	3–40	38	0.0010–0.0010	0.0010	3480.19–4099.07	–
(2 1 1 0 2 e)	3–64	61	0.0001–0.0010	0.0003	3313.30–4881.11	–
(2 1 1 0 2 f)	2–43	36	0.0002–0.0018	0.0006	3311.03–4026.46	–
(2 1 1 0 3 e)	8–54	47	0.0010–0.0016	0.0010	3181.03–4278.70	–
(2 1 1 1 1 e)	1–54	54	0.0002–0.0021	0.0003	5757.29–6872.67	–
(2 1 1 1 1 f)	1–55	54	0.0002–0.0016	0.0003	5757.29–6917.72	–
(2 1 1 1 2 e)	1–58	55	0.0002–0.0019	0.0003	5594.42–6877.41	–
(2 1 1 1 2 f)	1–59	56	0.0002–0.0017	0.0003	5594.42–6925.31	–
(2 1 1 1 3 e)	1–53	52	0.0002–0.0009	0.0003	5440.05–6515.50	–

(*continued on next page*)

Table 3 (*continued*).

Band	Range of J	No. of energy levels	Unc. range/hc cm^{-1}	Avg. unc./hc cm^{-1}	Range of energy levels/hc cm^{-1}	VBO/hc cm^{-1}
(2 1 1 1 3 *f*)	1–52	50	0.0002–0.0006	0.0002	5440.06–6478.73	–
(2 1 1 2 2 *e*)	7–33	11	0.0010–0.0010	0.0010	7874.90–8271.68	–
(2 1 1 2 2 *f*)	6–26	14	0.0010–0.0010	0.0010	7869.72–8116.90	–
(2 1 1 2 3 *e*)	8–31	13	0.0010–0.0010	0.0010	7726.90–8070.49	–
(2 1 1 2 3 *f*)	9–30	14	0.0010–0.0010	0.0010	7733.73–8048.40	–
(2 2 2 0 2 *e*)	21–39	12	0.0005–0.0008	0.0006	4151.00–4567.75	–
(2 2 2 0 2 *f*)	22–37	7	0.0005–0.0007	0.0006	4167.71–4509.34	–
(2 2 2 1 1 *e*)	5–33	24	0.0011–0.0013	0.0011	6449.03–6860.86	–
(2 2 2 1 1 *f*)	5–33	24	0.0011–0.0018	0.0012	6449.04–6860.90	–
(2 2 2 1 2 *e*)	4–35	32	0.0010–0.0014	0.0011	6255.24–6722.44	–
(2 2 2 1 2 *f*)	4–36	33	0.0011–0.0020	0.0012	6255.24–6749.56	–
(2 2 2 1 3 *e*)	7–27	18	0.0011–0.0012	0.0011	6085.98–6350.27	–
(2 2 2 1 3 *f*)	7–30	20	0.0011–0.0012	0.0011	6085.99–6415.92	–
(2 3 3 0 1 *e*)	13–31	16	0.0010–0.0011	0.0010	4928.64–5236.99	–
(2 3 3 0 1 *f*)	13–31	16	0.0011–0.0014	0.0011	4928.64–5236.99	–
(3 0 0 0 1 *e*)	8–24	14	0.0010–0.0020	0.0013	4221.81–4422.25	–
(3 0 0 0 2 *e*)	0–48	49	0.0001–0.0012	0.0004	4023.42–4912.80	4023.41806(120)
(3 0 0 0 3 *e*)	0–53	52	0.0001–0.0011	0.0003	3898.24–4978.33	3898.24483(71)
(3 0 0 0 4 *e*)	7–36	29	0.0003–0.0007	0.0004	3779.13–4263.43	–
(3 0 0 1 1 *e*)	0–65	65	0.0003–0.0014	0.0006	6463.48–8078.55	6463.47948(104)
(3 0 0 1 2 *e*)	0–75	70	0.0001–0.0010	0.0005	6298.11–8434.56	6298.11211(41)
(3 0 0 1 3 *e*)	0–71	68	0.0001–0.0030	0.0005	6175.95–8088.98	6175.95108(41)
(3 0 0 1 4 *e*)	1–60	56	0.0002–0.0010	0.0004	6034.23–7410.89	–
(3 1 1 0 1 *e*)	12–22	7	0.0020–0.0020	0.0020	4962.96–5095.61	–
(3 1 1 0 1 *f*)	14–22	5	0.0020–0.0020	0.0020	4983.80–5096.51	–
(3 1 1 0 2 *e*)	20–21	2	0.0021–0.0029	0.0025	4869.94–4885.82	–
(3 1 1 0 2 *f*)	24–24	1	0.0016–0.0016	0.0016	4938.88–4938.88	–
(3 1 1 0 3 *e*)	17–27	2	0.0011–0.0015	0.0013	4662.07–4832.22	–
(3 1 1 1 2 *e*)	2–41	35	0.0003–0.0030	0.0008	6974.98–7618.95	–
(3 1 1 1 2 *f*)	2–38	35	0.0003–0.0030	0.0009	6974.99–7530.91	–
(3 1 1 1 3 *e*)	4–40	34	0.0003–0.0021	0.0005	6818.40–7426.13	–
(3 1 1 1 3 *f*)	3–43	38	0.0003–0.0010	0.0005	6815.42–7523.04	–
(4 0 0 1 1 *e*)	5–40	30	0.0010–0.0018	0.0011	7883.74–8491.09	–
(4 0 0 1 2 *e*)	1–61	56	0.0010–0.0019	0.0010	7677.18–9097.15	–
(4 0 0 1 3 *e*)	0–46	47	0.0008–0.0011	0.0009	7525.82–8334.69	7525.82098(104)
(4 0 0 1 4 *e*)	0–61	52	0.0008–0.0010	0.0009	7397.76–8815.04	7397.75798(104)
(4 0 0 1 5 *e*)	2–46	41	0.0010–0.0021	0.0011	7233.13–8046.34	–
(4 1 1 0 4 *e*)	10–51	29	0.0010–0.0010	0.0010	5814.88–6775.33	–
(4 1 1 1 2 *e*)	3–46	33	0.0010–0.0014	0.0010	8368.77–9175.93	–
(4 1 1 1 2 *f*)	1–38	35	0.0010–0.0013	0.0010	8365.02–8923.23	–
(4 1 1 1 3 *e*)	2–47	38	0.0010–0.0021	0.0011	8186.03–9028.93	–
(4 1 1 1 3 *f*)	4–43	34	0.0010–0.0025	0.0011	8191.30–8895.49	–
(4 1 1 1 4 *e*)	6–40	18	0.0010–0.0010	0.0010	8032.80–8632.28	–
(4 1 1 1 4 *f*)	6–35	18	0.0010–0.0014	0.0010	8032.87–8491.81	–
(5 0 0 1 4 *e*)	8–43	19	0.0010–0.0010	0.0010	8775.60–9455.35	–

to be excluded from our final analysis. The 9822 unique measured transitions determine 5036 empirical rovibrational energy levels, extending up to 13 470 hc cm^{-1}. The average expanded uncertainty of the levels is 8×10^{-4} hc cm^{-1}.

Detailed comparisons of the empirical energy levels of the present study with their counterparts in the CDSD-296 [10] and the NASA Ames-2021 [13] databases reveal average differences of 0.0014 and 0.0165 hc cm^{-1}, respectively. Unlike other databases that rely heavily on theoretical calculations, our results are derived using the model-independent MARVEL algorithm, which ensures each energy level is supported by (often multiple) measured transitions. This approach can result in significantly lower uncertainties than calculations based on even refined potential energy surfaces, making them potentially more accurate and reliable than single experimental measurements. The MARVEL treatment is also easily extendable as new datasets of measured transitions can be added to the MARVEL input file and the procedure re-run; see Refs. [83] and [84] for recent examples.

CRediT authorship contribution statement

Saja A.M. Obaidat: Formal analysis, Data curation. **Ala'a A.A. Azzam:** Writing – original draft, Supervision, Data curation, Conceptualization. **Dunia Alatoom:** Writing – review & editing, Visualization, Formal analysis, Data curation. **Mohammad Taha I. Ibrahim:** Writing – review & editing, Visualization, Formal analysis, Data curation. **Jonathan Tennyson:** Writing – original draft, Project administration, Funding acquisition, Conceptualization. **Tibor Furtenbacher:** Writing – original draft, Software, Methodology, Investigation, Formal analysis, Data curation. **Attila G. Császár:** Writing – original draft, Methodology, Conceptualization.

Declaration of competing interest

The authors declare no conflict of interest.

Acknowledgments

The authors thank STFC for funding the UK–Jordan collaboration under the Newton Fund grant ST/T001429/1. JT acknowledges the support of the European Research Council (ERC) under the European Union's Horizon 2020 research and innovation programme through Advance Grant number 883830. The work of AGC and FT received support from NKFIH, Hungary (grant number K138233).

Appendix A. Supplementary data

Supplementary material related to this article can be found online at https://doi.org/10.1016/j.jqsrt.2025.109444.

Data availability

The MARVEL input file, including all the transitions, and the MARVEL output file, with all the energy levels, are supplied as Supplementary Material to this paper. Both the measured transitions and the empirical energy levels have expanded (two-sigma) uncertainties attached to them.

References

[1] Gordon IE, Rothman LS, Hargreaves RJ, Hashemi R, Karlovets EV, Skinner FM, et al. The HITRAN2020 molecular spectroscopic database. J Quant Spectrosc Radiat Transfer 2022;277:107949. http://dx.doi.org/10.1016/j.jqsrt.2021.107949.

[2] Bernath PF, McElroy CT, Abrams MC, Boone CD, Butler M, Camy-Peyret C, et al. Atmospheric chemistry experiment (ACE): Mission overview. Geophys Res Lett 2025;32:L15S01. http://dx.doi.org/10.1029/2005gl022386.

[3] Butz A, Guerlet S, Hasekamp O, Schepers D, Galli A, Aben I, et al. Toward accurate CO_2 and CH_4 observations from GOSAT. Geophys Res Lett 38. http://dx.doi.org/10.1029/2011gl047888.

[4] Eldering A, Taylor TE, O'Dell CW, Pavlick R. The OCO-3 mission: measurement objectives and expected performance based on 1 year of simulated data. Atmos. Meas Techn. 2019;12:2341–70. http://dx.doi.org/10.5194/amt-12-2341-2019.

[5] Hobbs JM, Drouin BJ, Oyafuso F, Payne VH, Gunson MR, McDuffie J, et al. Spectroscopic uncertainty impacts on OCO-2/3 retrievals of XCO_2. J Quant Spectrosc Rad. Transf 2020;257:107360. http://dx.doi.org/10.1016/j.jqsrt.2020.107360.

[6] Thorpe AK, Green RO, Thompson DR, Brodrick PG, Chapman JW, Elder CD, et al. Attribution of individual methane and carbon dioxide emission sources using EMIT observations from space. Sci Adv 2023;9:eadh2391. http://dx.doi.org/10.1126/sciadv.adh2391.

[7] Ward JK, Strain BR. Elevated CO_2 studies: past, present and future. Tree Physiol 1999;19:211–20. http://dx.doi.org/10.1093/treephys/19.4-5.211.

[8] Perevalov BV, Kassi S, Perevalov VI, Tashkun SA, Campargue A. High sensitivity CW-CRDS spectroscopy of $^{12}C^{16}O_2$,$^{16}O^{12}C^{17}O$ and $^{16}O^{12}C^{18}O$ between 5851 and 7045 cm^{-1}: Line positions analysis and critical review of the current databases. J Mol Spectrosc 2008;252:143–59. http://dx.doi.org/10.1016/j.jms.2008.06.012.

[9] Galli I, Bartalini S, Ballerini R, Barucci M, Cancio P, De Pas M, et al. Spectroscopic detection of radiocarbon dioxide at parts-per-quadrillion sensitivity. Optica 2016;3:385. http://dx.doi.org/10.1364/optica.3.000385.

[10] Tashkun SA, Perevalov VI, Gamache RR, Lamouroux J. CDSD-296, high-resolution carbon dioxide spectroscopic databank: An update. J Quant Spectrosc Radiat Transfer 2019;228:124–31. http://dx.doi.org/10.1016/j.jqsrt.2019.03.001.

[11] Yurchenko SN, Mellor TM, Freedman RS, Tennyson J. ExoMol line lists – XXXIX. Ro-vibrational molecular line list for CO_2. Mon Not R Astron Soc 2020;496:5282–91. http://dx.doi.org/10.1093/mnras/staa1874.

[12] Delahaye T, Armante R, Scott N, Jacquinet-Husson N, Chédin A, Crépeau L, et al. The 2020 edition of the GEISA spectroscopic database. J Mol Spectrosc 2021;380:111510.

[13] Huang X, Schwenke DW, Freedman RS, Lee TJ. Ames-2021 CO_2 dipole moment surface and IR line lists: Toward 0.1% uncertainty for CO_2 IR intensities. J Phys Chem A 2022;126:5940–64. http://dx.doi.org/10.1021/acs.jpca.2c01291.

[14] Ibrahim MTI, Alatoom D, Furtenbacher T, Császár AG, Yurchenko SN, Azzam AAA, et al. MARVEL analysis of high-resolution rovibrational spectra of$^{13}C^{16}O_2$. J Comput Chem 2024;45:969–84. http://dx.doi.org/10.1002/jcc.27266.

[15] Alatoom D, Ibrahim MTI, Furtenbacher T, Császár AG, Alghizzawi M, Yurchenko SN, et al. MARVEL analysis of high-resolution rovibrational spectra of$^{16}O^{12}C^{18}O$. J Comput Chem 2024;45:2558–73. http://dx.doi.org/10.1002/jcc.27453.

[16] Azzam AAA, Azzam SAA, Aburumman KAA, Tennyson J, Yurchenko SN, Császár AG, et al. MARVEL analysis of high-resolution rovibrational spectra of the$^{18}O^{12}C^{18}O$,$^{17}O^{12}C^{18}O$, and$^{18}O^{13}C^{18}O$ isotopologues of carbon dioxide. J Mol Spectrosc 2024;405:111947. http://dx.doi.org/10.1016/j.jms.2024.111947.

[17] Azzam AAA, Tennyson J, Yurchenko SN, Furtenbacher T, Császár AG. MARVEL analysis of high-resolution rovibrational spectra of$^{16}O^{13}C^{18}O$. J Comput Chem 2025;46:e27541. http://dx.doi.org/10.1002/jcc.27541.

[18] Azzam AAA, Abou Doud BMJ, Shersheer MQA, Almasri BKM, Bader CNM, Baraa AMHA, et al. MARVEL analysis of high-resolution rovibrational spectra of$^{16}O^{12}C^{16}O$. Sci Data 2025;12:532. http://dx.doi.org/10.1038/s41597-025-04755-w.

[19] JWST Transiting Exoplanet Community Early Release Science Team. Identification of carbon dioxide in an exoplanet atmosphere. Nature 2023;614:649–52. http://dx.doi.org/10.1038/s41586-022-05269-w.

[20] Bertaux J-L, Vandaele AC, Wilquet V, Montmessin F, Dahoo R, Villard E, et al. First observation of 628 CO_2 isotopologue band at 3.3 μm in the atmosphere of Venus by solar occultation from Venus express. Icarus 2008;195:28–33. http://dx.doi.org/10.1016/j.icarus.2008.01.001.

[21] Webster CR, Mahaffy PR, Flesch GJ, Niles PB, Jones JH, Leshin LA, et al. Isotope ratios of H, C, and O in CO_2 and H_2O of the Martian atmosphere. Science 2013;341:260–3. http://dx.doi.org/10.1126/science.1237961.

[22] Ahrer E-M, Alderson L, Batalha NM, Batalha NE, Bean JL, Beatty TG, et al. Identification of carbon dioxide in an exoplanet atmosphere. Nature 2023;614:649–52. http://dx.doi.org/10.1038/s41586-022-05269-w.

[23] Baldacci A, Malathy Devi V, Chen D-W, Narahari Rao K, Fridovich B. Absorption spectrum of carbon dioxide at 4.3 μm. J Mol Spectrosc 1978;70:143–59. http://dx.doi.org/10.1016/0022-2852(78)90016-4.

[24] Guelachvili G. High-resolution Fourier spectra of carbon dioxide and three of its isotopic species near 4.3 μm. J Mol Spectrosc 1980;79:72–83. http://dx.doi.org/10.1016/0022-2852(80)90293-3.

[25] Paso R, Kauppinen J, Anttila R. Infrared spectrum of CO_2 in the region of the bending fundamental ν_2. J Mol Spectrosc 1980;79:236–53. http://dx.doi.org/10.1016/0022-2852(80)90304-5.

[26] Rinsland CP, Benner DC. Absolute intensities of spectral lines in carbon dioxide bands near 2050 cm^{-1}. Appl Opt 1984;23:4523–8. http://dx.doi.org/10.1364/AO.23.004523.

[27] Rinsland CP, Benner DC, Devi VM. Absolute line intensities in CO_2 bands near 4.8 μm. Appl Opt 1986;25:1204–14. http://dx.doi.org/10.1364/AO.25.001204.

[28] Claveau C, Teffo J-L, Hurtmans D, Valentin A, Gamache RR. Line positions and absolute intensities in the laser bands of carbon-12 oxygen-17 isotopic species of carbon dioxide. J Mol Spectrosc 1999;193:15–32. http://dx.doi.org/10.1006/jmsp.1998.7704.

[29] Lyulin OM, Karlovets EV, Jacquemart D, Lu Y, Liu AW, Perevalov VI. Infrared spectroscopy of ^{17}O- and ^{18}O-enriched carbon dioxide in the 1700–8300 cm^{-1} wavenumber region. J Quant Spectrosc Radiat Transfer 2012;113:2167–81. http://dx.doi.org/10.1016/j.jqsrt.2012.06.028.

[30] Rinsland CP, Benner DC, Devi VM, Ferry PS, Sutton CH, Richardson DJ. Atlas of high resolution infrared spectra of carbon dioxide. Appl Opt 1984;23:2051–2. http://dx.doi.org/10.1364/AO.23.002051.

[31] Jacquemart D, Gueye F, Lyulin OM, Karlovets EV, Baron D, Perevalov VI. Infrared spectroscopy of CO_2 isotopologues from 2200 to 7000 cm^{-1}: I—Characterizing experimental uncertainties of positions and intensities. J Quant Spectrosc Radiat Transfer 2012;113:961–75. http://dx.doi.org/10.1016/j.jqsrt.2012.02.020.

[32] Rinsland CP, Benner DC, Devi VM. Measurements of absolute line intensities in carbon dioxide bands near 5.2 μm. Appl Opt 1985;24:1644–50. http://dx.doi.org/10.1364/AO.24.001644.

[33] Elliott BM, Sung K, Miller CE. FT-IR spectra of^{17}O-enriched CO_2 in the ν_3 region: High accuracy frequency calibration and spectroscopic constants for $^{16}O^{12}C^{17}O$, $^{17}O^{12}C^{17}O$, and $^{17}O^{12}C^{18}O$. J Mol Spectrosc 2014;304:1–11. http://dx.doi.org/10.1016/j.jms.2014.08.001.

[34] Devi VM, Rinsland CP, Benner DC. Absolute intensity measurements of CO_2 bands in the 2395–2680-cm^{-1} region. Appl Opt 1984;23:4067. http://dx.doi.org/10.1364/AO.23.004067.

[35] Villanueva GL, Mumma MJ, Novak RE, Hewagama T. Identification of a new band system of isotopic CO_2 near 3.3 μm: Implications for remote sensing of biomarker gases on Mars. Icarus 2008;195:34–44. http://dx.doi.org/10.1016/j.icarus.2007.11.014.

[36] Borkov YG, Jacquemart D, Lyulin OM, Tashkun SA, Perevalov VI. Infrared spectroscopy of^{17}O- and ^{18}O-enriched carbon dioxide: Line positions and intensities in the 3200–4700 cm^{-1} region. Global modeling of the line positions of $^{16}O^{12}C^{17}O$ and $^{17}O^{12}C^{17}O$. J Quant Spectrosc Radiat Transfer 2014;137:57–76. http://dx.doi.org/10.1016/j.jqsrt.2013.11.008.

[37] Vasilchenko S, Konefal M, Mondelain D, Kassi S, Čermák P, Tashkun SA, et al. The CO_2 absorption spectrum in the 2.3 μm transparency window by high sensitivity CRDS: (I) Rovibrational lines. J Quant Spectrosc Radiat Transfer 2016;184:233–40. http://dx.doi.org/10.1016/j.jqsrt.2016.07.002.

[38] Borkov YG, Jacquemart D, Lyulin OM, Tashkun SA, Perevalov VI. Infrared spectroscopy of ^{17}O- and ^{18}O-enriched carbon dioxide: Line positions and intensities in the 4681–5337 cm^{-1} region. J Quant Spectrosc Radiat Transfer 2015;159:1–10. http://dx.doi.org/10.1016/j.jqsrt.2015.02.019.

[39] Benner DC, Devi VM, Sung K, Brown LR, Miller CE, Payne VH, et al. Line parameters including temperature dependences of air- and self-broadened line shapes of $^{12}C^{16}O_2$: 2.06-μm region. J Mol Spectrosc 2016;326:21–47. http://dx.doi.org/10.1016/j.jms.2016.02.012.

[40] Mondelain D, Karlovets E, Perevalov V, Tashkun S, Campargue A. High-sensitivity CRDS absorption spectrum of ^{17}O enriched carbon dioxide near 1.74 μm. J Mol Spectrosc 2019;362:84–9. http://dx.doi.org/10.1016/j.jms.2019.06.004.

[41] Karlovets EV, Čermák P, Mondelain D, Kassi S, Campargue A, Tashkun SA, et al. Analysis and theoretical modeling of the ^{18}O enriched carbon dioxide spectrum by CRDS near 1.74 μm. J Quant Spectrosc Radiat Transfer 2018;217:73–85. http://dx.doi.org/10.1016/j.jqsrt.2018.05.017.

[42] Čermák P, Karlovets EV, Mondelain D, Kassi S, Perevalov VI, Campargue A. High sensitivity CRDS of CO_2 in the 1.74 μm transparency window. A validation test for the spectroscopic databases. J Quant Spectrosc Radiat Transfer 2018;207:95–103. http://dx.doi.org/10.1016/j.jqsrt.2017.12.018.

[43] Jacquemart D, Borkov Y, Lyulin O, Tashkun S, Perevalov V. Fourier transform spectroscopy of CO_2 isotopologues at 1.6 μm: Line positions and intensities. J Quant Spectrosc Radiat Transfer 2015;160:1–9. http://dx.doi.org/10.1016/j.jqsrt.2015.03.016.

[44] Karlovets EV, Campargue A, Mondelain D, Kassi S, Tashkun SA, Perevalov VI. High sensitivity cavity ring down spectroscopy of ^{18}O enriched carbon dioxide between 5850 and 7000 cm^{-1}: Part II. Analysis and theoretical modeling of the $^{12}C^{18}O_2$, $^{13}C^{18}O_2$ and $^{16}O^{13}C^{18}O$ spectra. J Quant Spectrosc Radiat Transfer 2014;136:71–88. http://dx.doi.org/10.1016/j.jqsrt.2013.11.005.

[45] Perevalov BV, Kassi S, Romanini D, Perevalov VI, Tashkun SA, Campargue A. CW-cavity ringdown spectroscopy of carbon dioxide isotopologues near 1.5 μm. J Mol Spectrosc 2006;238:241–55. http://dx.doi.org/10.1016/j.jms.2006.05.009.

[46] Majcherova Z, Macko P, Romanini D, Perevalov VI, Tashkun SA, Teffo J-L, et al. High-sensitivity CW-cavity ringdown spectroscopy of $^{12}CO_2$ near 1.5 μm. J Mol Spectrosc 2005;230:1–21. http://dx.doi.org/10.1016/j.jms.2004.09.011.

[47] Kassi S, Karlovets EV, Tashkun SA, Perevalov VI, Campargue A. Analysis and theoretical modeling of the ^{18}O enriched carbon dioxide spectrum by CRDS near 1.35 μm: (I) $^{16}O^{12}C^{18}O$, $^{16}O^{12}C^{17}O$, $^{12}C^{16}O_2$ and $^{13}C^{16}O_2$. J Quant Spectrosc Radiat Transfer 2017;187:414–25. http://dx.doi.org/10.1016/j.jqsrt.2016.09.002.

[48] Kassi S, Song KF, Campargue A. High sensitivity CW-cavity ring down spectroscopy of $^{12}CO_2$ near 1.35 μm (I): line positions. J Quant Spectrosc Radiat Transfer 2009;110:1801–14. http://dx.doi.org/10.1016/j.jqsrt.2009.04.010.

[49] Song KF, Kassi S, Tashkun SA, Perevalov VI, Campargue A. High sensitivity CW-cavity ring down spectroscopy of $^{12}CO_2$ near 1.35 μm (II): New observations and line intensities modeling. J Quant Spectrosc Radiat Transfer 2010;111:332–44. http://dx.doi.org/10.1016/j.jqsrt.2009.09.004.

[50] Karlovets EV, Kassi S, Tashkun SA, Perevalov VI, Campargue A. High sensitivity cavity ring down spectroscopy of carbon dioxide in the 1.19–1.26 μm region. J Quant Spectrosc Radiat Transfer 2014;144:137–53. http://dx.doi.org/10.1016/j.jqsrt.2014.04.001.

[51] Golebiowski D, Herman M, Lyulin O.$^{16}O^{12}C^{17}O$ and $^{18}O^{12}C^{17}O$ spectroscopy in the 1.2–1.25 μm region. Can J Phys 2013;91:963–5. http://dx.doi.org/10.1139/cjp-2012-0482.

[52] Pan H, Li X-F, Lu Y, Liu A-W, Perevalov V, Tashkun S, et al. Cavity ring down spectroscopy of ^{18}O and ^{17}O enriched carbon dioxide near 795 nm. J Quant Spectrosc Radiat Transfer 2013;114:42–4. http://dx.doi.org/10.1016/j.jqsrt.2012.08.017.

[53] Shine KP, Perry GE. Radiative forcing due to carbon dioxide decomposed into its component vibrational bands. Q J R. Meteorol 2023;149(754):1856–66. http://dx.doi.org/10.1002/qj.4485.

[54] Császár AG, Czakó G, Furtenbacher T, Mátyus E. An active database approach to complete rotational–vibrational spectra of small molecules. Annu Rep Comput Chem 2007;3:155–76.

[55] Furtenbacher T, Császár AG, Tennyson J. MARVEL: measured active rotational-vibrational energy levels. J Mol Spectrosc 2007;245:115–25. http://dx.doi.org/10.1016/j.jms.2007.07.005.

[56] Furtenbacher T, Császár AG. MARVEL: measured active rotational-vibrational energy levels. II. Algorithmic improvements. J Quant Spectrosc Radiat Transfer 2012;113:929–35. http://dx.doi.org/10.1016/j.jqsrt.2012.01.005.

[57] Császár AG, Furtenbacher T, Árendás P. Small molecules – big data. J Phys Chem A 2016;120:8949–69. http://dx.doi.org/10.1021/acs.jpca.6b02293.

[58] Tóbiás R, Furtenbacher T, Tennyson J, Császár AG. Accurate empirical rovibrational energies and transitions of $H_2{}^{16}O$. Phys Chem Chem Phys 2019;21:3473–95. http://dx.doi.org/10.1039/c8cp05169k.

[59] Császár AG, Furtenbacher T. Spectroscopic networks. J Mol Spectrosc 2011;266:99–103. http://dx.doi.org/10.1016/j.jms.2011.03.031.

[60] Furtenbacher T, Császár AG. The role of intensities in determining characteristics of spectroscopic networks. J Mol Struct 2012;1009:123–9. http://dx.doi.org/10.1016/j.molstruc.2011.10.057.

[61] Gordon IE, Rothman LS, Hargreaves RJ, Hashemi R, Karlovets EV, Skinner FM, et al. The HITRAN2020 molecular spectroscopic database. J Quant Spectrosc Radiat Transfer 2022;277:107949. http://dx.doi.org/10.1016/j.jqsrt.2021.107949.

[62] Huang X, Schwenke DW, Lee TJ. Isotopologue consistency of semi-empirically computed infrared line lists and further improvement for rare isotopologues: CO_2 and SO_2 case studies. J Quant Spectrosc Radiat Transfer 2019;230:222–46. http://dx.doi.org/10.1016/j.jqsrt.2019.03.002.

[63] Tennyson J, Yurchenko SN, Zhang J, Bowesman CA, Brady RP, Buldyreva J, et al. The 2024 release of the ExoMol database: molecular line lists for exoplanet and other hot atmospheres. J Quant Spectrosc Radiat Transfer 2024;326:109083. http://dx.doi.org/10.1016/j.jqsrt.2024.109083.

[64] Tennyson J, Furtenbacher T, Yurchenko SN, Császár AG. Empirical rovibrational energy levels for nitrous oxide. J Quant Spectrosc Radiat Transfer 2024;316:108902. http://dx.doi.org/10.1016/j.jqsrt.2024.108902.

[65] Furtenbacher T, Tóbiás R, Tennyson J, Polyansky OL, Császár AG. W2020: A database of validated rovibrational experimental transitions and empirical energy levels of $H_2{}^{16}O$. J Phys Chem Ref Data 2020;49:033101. http://dx.doi.org/10.1063/5.0008253.

[66] Ritz W. On a new law of series spectra. Astrophys J 1908;28:237–43. http://dx.doi.org/10.1086/141591.

[67] Amat G, Pimbert M. On Fermi resonance in carbon dioxide. J Mol Spectrosc 1965;16:278–90. http://dx.doi.org/10.1016/0022-2852(65)90123-2.

[68] Rothman LS, Young LDG. Infrared energy levels and intensities of carbon dioxide—II. J Quant Spectrosc Radiat Transfer 1981;25:505–24. http://dx.doi.org/10.1016/0022-4073(81)90026-1.

[69] Toth RA, Brown LR, Miller CE, Malathy Devi V, Benner DC. Spectroscopic database of CO_2 line parameters: $4300-7000$ cm^{-1}. J Quant Spectrosc Radiat Transfer 2008;109:906–21. http://dx.doi.org/10.1016/j.jqsrt.2007.12.004.

[70] McClatchey RA, Benedict WS, Clough SA, Burch DE, Calfee RF, Fox K, et al. AFCRL Atmospheric Absorption Line Parameters Compilation. Tech. Rep. AFCRL-TR-73-0096, Air Force Cambridge Research Laboratories; 1983, https://modis-images.gsfc.nasa.gov/JavaHAWKS/AFCRL_AALPC.pdf.

[71] Baldacci A, Rinsland CP, Smith MAH, Rao KN. Spectrum of $^{13}C^{16}O_2$ at 2.8 μm. J Mol Spectrosc 1982;94:351–62. http://dx.doi.org/10.1016/0022-2852(82)90011-X.

[72] McCoy AB, Sibert EL. Perturbative calculations of vibrational ($J = 0$) energy levels of linear molecules in normal coordinate representations. J Chem Phys 1991;95:3476–87. http://dx.doi.org/10.1063/1.460850.

[73] Cerezo J, Bastida A, Requena A, Zúñiga J. Rovibrational energies, partition functions and equilibrium fractionation of the CO_2 isotopologues. J Quant Spectrosc Rad. Transf 2014;147:233–51. http://dx.doi.org/10.1016/j.jqsrt.2014.06.003.

[74] Lemus R, Sánchez-Castellanos M, Pérez-Bernal F, Fernández JM, Carvajal M. Simulation of the Raman spectra of CO_2: Bridging the gap between algebraic models and experimental spectra. J Chem Phys 2014;141:054306. http://dx.doi.org/10.1063/1.4889995.

[75] Bermudez-Montaña M, Lemus R, Pérez-Bernal F, Carvajal M. Comprehensive vibrational analysis of CO_2 based on a polyad-preserving model. Eur Phys J D 2017;71:147. http://dx.doi.org/10.1140/epjd/e2017-80178-6.

[76] Brown JM, Hougen JT, Huber KP, Johns JWC, Kopp I, Lefebvre-Brion H, et al. Labeling of parity doublet levels in linear molecules. J Mol Spectrosc 1975;55:500–3. http://dx.doi.org/10.1016/0022-2852(75)90291-X.

[77] Esplin MP, Huppi RJ, Sakai H, Vanasse GA, Rothman LS. Absorption Measurements of CO_2 and H_2O at High Resolution and Elevated Temperatures. Tech. Rep. AFGL-TR-82-0057, Utah State University; 1982, https://apps.dtic.mil/sti/citations/ADA113824.

[78] Tashkun SA, Perevalov VI, Gamache RR, Lamouroux J. CDSD-296, high-resolution carbon dioxide spectroscopic databank: An update. J Quant Spectrosc Radiat Transfer 2019;228:124–31. http://dx.doi.org/10.1016/j.jqsrt.2019.03.001.

[79] Pickett HM, Poynter RL, Cohen EA, Delitsky ML, Pearson JC, Müller HSP. Submillimeter, millimeter, and microwave spectral line catalog. J Quant Spectrosc Radiat Transfer 1998;60:883–90. http://dx.doi.org/10.1016/S0022-4073(98)00091-0.

[80] Zak EJ, Tennyson J, Polyansky OL, Lodi L, Zobov NF, Tashkun SA, et al. Room temperature line lists for CO_2 asymmetric isotopologues with *ab initio* computed intensities. J Quant Spectrosc Radiat Transfer 2017;203:265–81. http://dx.doi.org/10.1016/j.jqsrt.2017.01.037.

[81] Newman MEJ. Networks. Oxford: Oxford University Press; 2010.

[82] Furtenbacher T, Árendás P, Mellau G, Császár AG. Simple molecules as complex systems. Sci Rep 2014;4:4654. http://dx.doi.org/10.1038/srep04654.

[83] McKemmish LK, Syme A-M, Borsovszky J, Yurchenko SN, Tennyson J, Furtenbacher T, et al. An update to the MARVEL data set and ExoMol line list for $^{12}C_2$. Mon Not R Astron Soc 2020;497:1081–97. http://dx.doi.org/10.1093/mnras/staa1954.

[84] Germann M, Hjalten A, Tennyson J, Yurchenko SN, Gordon IE, Pett C, et al. Optical frequency comb Fourier transform spectroscopy of formaldehyde in the 1250 to 1390 cm^{-1} range: experimental line list and MARVEL analysis. J Quant Spectrosc Radiat Transfer 2024;312:108782. http://dx.doi.org/10.1016/j.jqsrt.2023.108782.